TU Delft

Delft University of Technology

Document Version
Final published version

Licence
Dutch Copyright Act (Article 25fa)

Citation (APA)
Liang, J., Fan, J., Zhang, G., & Van Driel, W. D. (2026). A Multi-Agent System for Automated Lifetime Prediction of Power Electronics. In *Proceedings - 2026 27th International Conference on Thermal, Mechanical and Multi-Physics Simulation and Experiments in Microelectronics and Microsystems, EuroSimE 2026* (Proceedings - 2026 27th International Conference on Thermal, Mechanical and Multi-Physics Simulation and Experiments in Microelectronics and Microsystems, EuroSimE 2026). IEEE. https://doi.org/10.1109/EuroSimE69483.2026.11511926

Important note
To cite this publication, please use the final published version (if applicable).
Please check the document version above.

Copyright
In case the licence states “Dutch Copyright Act (Article 25fa)”, this publication was made available Green Open Access via the TU Delft Institutional Repository pursuant to Dutch Copyright Act (Article 25fa, the Taverne amendment). This provision does not affect copyright ownership.
Unless copyright is transferred by contract or statute, it remains with the copyright holder.

Sharing and reuse
Other than for strictly personal use, it is not permitted to download, forward or distribute the text or part of it, without the consent of the author(s) and/or copyright holder(s), unless the work is under an open content license such as Creative Commons.

Takedown policy
Please contact us and provide details if you believe this document breaches copyrights.
We will remove access to the work immediately and investigate your claim.

This work is downloaded from Delft University of Technology.

A Multi-Agent Digital Twin Framework for Health Monitoring of SiC MOSFETs in Power Converters

1st Alireza Mehrabi
Department of Microelectronics
Delft University of Technology
Delft, the Netherlands
a.mehrabi@tudelft.nl

2nd Zihan Zhang
Department of Microelectronics
Delft University of Technology
Delft, the Netherlands
z.zhang-6@tudelft.nl

3rd Filip Simjanoski
Department of Microelectronics
Delft University of Technology
Delft, the Netherlands
f.simjanoski@tudelft.nl

4th Rene H. Poelma
Department of Microelectronics
Delft University of Technology
Delft, the Netherlands
r.h.poelma@tudelft.nl

5th Willem D. van Driel
Department of Microelectronics
Delft University of Technology
Delft, the Netherlands
Willem.vanDriel@tudelft.nl

6th Guo Qi Zhang
Department of Microelectronics
Delft University of Technology
Delft, the Netherlands
g.q.zhang@tudelft.nl

2026 27th International Conference on Thermal, Mechanical and Multi-Physics Simulation and Experiments in Microelectronics and Microsystems (EuroSimE) | 979-8-3315-6249-6/26/$31.00 ©2026 IEEE | DOI: 10.1109/EuroSimE69483.2026.11511969

***Abstract*—Modeling and monitoring advanced power semiconductor packages are challenging due to their multiphysics behavior, structural complexity, and the high computational cost associated with detailed models. Conventional high-fidelity approaches, such as finite element models, provide high accuracy but are often unsuitable for applications like health monitoring, while purely data-driven models may lack physical interpretability and robustness under degradation.**

This paper proposes the concept of a multi-agent digital twin framework to address these challenges by decomposing the overall system into interconnected virtual domains with different roles and fidelity levels. The approach is demonstrated for health monitoring of a SiC MOSFET in a DC–DC buck converter. A three-agent architecture is implemented, consisting of a temporal ANN for system identification, a decision layer for failure detection and localization, and a parametric reduced-order thermal model for failure assessment. Experimental results show that the proposed framework can accurately identify system behavior, detect and localize failures, and quantify parameter variations associated with degradation.

***Index Terms*—Digital Twin, AI, Power Semiconductors, Buck Converter, SiC MOSFET.**

I. Introduction

The rapid growth in the complexity of advanced power semiconductor packaging has increased the need for more advanced simulation methods. These methods should be able to detect weaknesses in package design and address reliability concerns. For years, finite element models have been known as high-fidelity models for electrical, thermal, and mechanical simulation of packages [1]–[4]. While they provide significant flexibility for designers to evaluate new design solutions and for reliability engineers to simulate possible failures, their high computational cost and extensive information requirements limit their applicability in certain cases, such as health monitoring and simulation of device operation under real operating conditions. This has led to increasing interest in alternative methods such as Parametric Reduced Order Models (PROMs).

Small-signal models of switches can be defined as PROMs and can be used to describe the electrical behavior of the switches and changes in the health state of the packages, where the parasitic resistance, capacitance, and inductance of electrical paths, such as gate-to-source or drain-to-source, are mapped to single values [5]. In addition, Lumped Parameter Thermal Networks (LPTNs) can be used as PROMs to describe the thermal behavior of semiconductor packages, where thermal properties of materials at different levels are represented [6]. As a solution for monitoring mechanical properties such as stress and strain in power electronic packages, especially in power converters and PCBs, System Equivalent Reduction and Expansion Process (SEREP) is an effective approach in which the mechanical and dynamic parameters are reduced at specific locations, e.g., sensor locations, and then expanded back to the full structure to monitor variations [7]. Although the application of these methods in various studies demonstrates their benefits, all of them can be categorized as model-based monitoring methods, and require accurate device information.

On the other hand, non-model-based methods, such as artificial neural networks (ANNs), are commonly used as PROMs. These models, also known as black-box or data-driven models, map the relationship between device inputs, such as input load, and measurable package parameters, such as temperature. Although they require a large amount of training data to achieve generalization, they are capable of capturing the nonlinear and dynamic behavior of devices [8]. Nevertheless, similar to model-based approaches, they have limited ability to predict device behavior after degradation occurs, as they are typically trained on intact devices, and hardware-based simulation of complex failures can be too complicated to generate sufficient training data under failed conditions.

Digital twin modeling, as an advanced modeling technique, is another solution for monitoring power semiconductor devices. A digital twin is defined as a virtual representation

979-8-3315-6249-6/26/$31.00 ©2026 IEEE Authorized licensed use limited to: TU Delft Library. Downloaded on July 13,2026 at 13:04:58 UTC from IEEE Xplore. Restrictions apply.

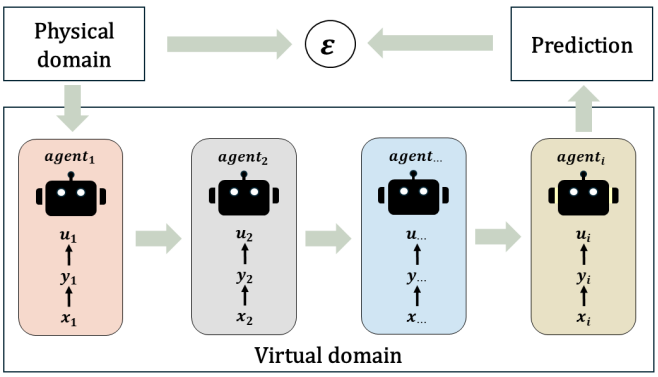


Fig. 1: Example of a sequential multi-agent digital twin illustrating the interaction between interconnected virtual domains and the pyhsical domain.

of a real element, where the representation is continuously optimized to accurately mimic the behavior of its physical counterpart. Depending on the target application, digital twin modeling, prediction, and optimization can be complex. The model may be multiscale, multiphysics, or probabilistic, or it may be a PROM that is optimized over time [9], [10]. However, as discussed previously, modeling and optimization are not always straightforward tasks.

To overcome this challenge, this work proposes the concept of a multi-agent digital twin. A multi-agent digital twin represents a physical element in separate virtual domains that are connected sequentially or hierarchically, where a specific task, physical aspect, or level of fidelity is assigned to each domain.

II. Multi-Agent Digital Twin: Definition

A multi-agent digital twin is a way of representing a physical element as separate virtual domains that are connected sequentially or hierarchically and linked through decisions made by the agent of each domain. Each domain can represent a physical aspect, a specific task within a broader objective, or a different fidelity level. The multi-agent concept simplifies digital twin modeling and reduces complexity because, instead of solving one large problem, it divides the system into smaller tasks with different fidelity levels. The proposed multi-agent digital twin can be formally represented as a structured probabilistic graphical model:

$$\begin{aligned} p(x_p, \{x_i\}|\{y_i\}) \propto p(x_p) \prod_i p(y_i|x_i) p(x_i|x_p) \\ p(u_i|x_i, y_i, \{u_j\}_{j\in Pa(i)}) \prod_{(j\to i)\in\epsilon} p(x_i|x_j) \end{aligned} \tag{1}$$

where,
x_p: is the current state of the physical system,
x_i: is the current state of the virtual domain i, where $i = 1, 2, ...n$,
y_i: is the observation inside domain i, such as a simulation output, predicted value, or sensor measurement,
u_i: is the agent's decision in domain i.

In this formulation, the joint probability of the physical system state, the set of virtual domain states, and the agent decision variables, conditioned on the available observations, is expressed as a combination of several components. The prior term $p(x_p)$ represents the initial knowledge, physical laws, or structural constraints of the underlying physical system. The likelihood terms $p(y_i|x_i)$ describe how observations within each virtual domain relate to its internal state, reflecting the local inference performed by individual agents. The terms $p(x_i|x_p)$ and $p(x_i|x_j)$ model the coupling between the physical system and its virtual representations, as well as the dependencies among interconnected domains through sequential or hierarchical relationships. The decision term $p(u_i|x_i, y_i, \{u_j\}_{j\in Pa(i)})$ represents how each agent selects actions or control inputs based on its local state, its observations, and information received from connected agents. Together, these components maintain global consistency of the digital twin while preserving modularity, local autonomy, and scalable decision-making across multiple virtual domains. A flowchart of a sequential multi-agent digital twin is shown in Fig. 1.

To provide a clearer understanding of this concept, a multi-agent digital twin is used in this paper for the health monitoring of a DC–DC buck converter to detect, localize, and assess failures. Designing a single large model capable of performing all these tasks would require extensive simulations, large datasets, and numerous experiments. This example demonstrates how a multi-agent digital twin can divide this large problem into smaller tasks while maintaining a high level of accuracy.

III. Multi-Agent Digital Twin: Real Application

As an application of the proposed concept, a commercially available 300 W, 20 A step-down DC–DC buck converter was used as the system, and the health state of the SiC MOSFET switch in this converter was monitored. A Keithley 2561A high-power source was connected to the converter with voltage and current limits of 10 V and 15 A to provide the input power. At the output, a Keithley 2380 DC Electronic Load (120 V, 60 A, 250 W) was connected. To control the load, the DC load was connected to a PC via a USB cable and controlled using MATLAB. To measure the temperature, a K-type thermocouple was attached to the back of the MOSFET and connected to an Arduino UNO via a MAX31856 thermocouple amplifier with a resolution of $0.0078125\ ^oC$. For cooling, the converter was connected to a cold plate on the backside of the MOSFET. Fig.2 shows the test setup.

The temperature measured by the thermocouple (T_{case}), the applied load (I_L), and the power loss of the system (P_{loss}) were considered as the links from the physical system to the virtual domains, i.e., the multi-agent digital twin.

A complete digital twin algorithm for health monitoring should be able to cover three steps. First, it needs to detect failures. Then, the source of the failure should be identified, and finally, the failure must be assessed or quantified. One

Authorized licensed use limited to: TU Delft Library. Downloaded on July 13,2026 at 13:04:58 UTC from IEEE Xplore. Restrictions apply.

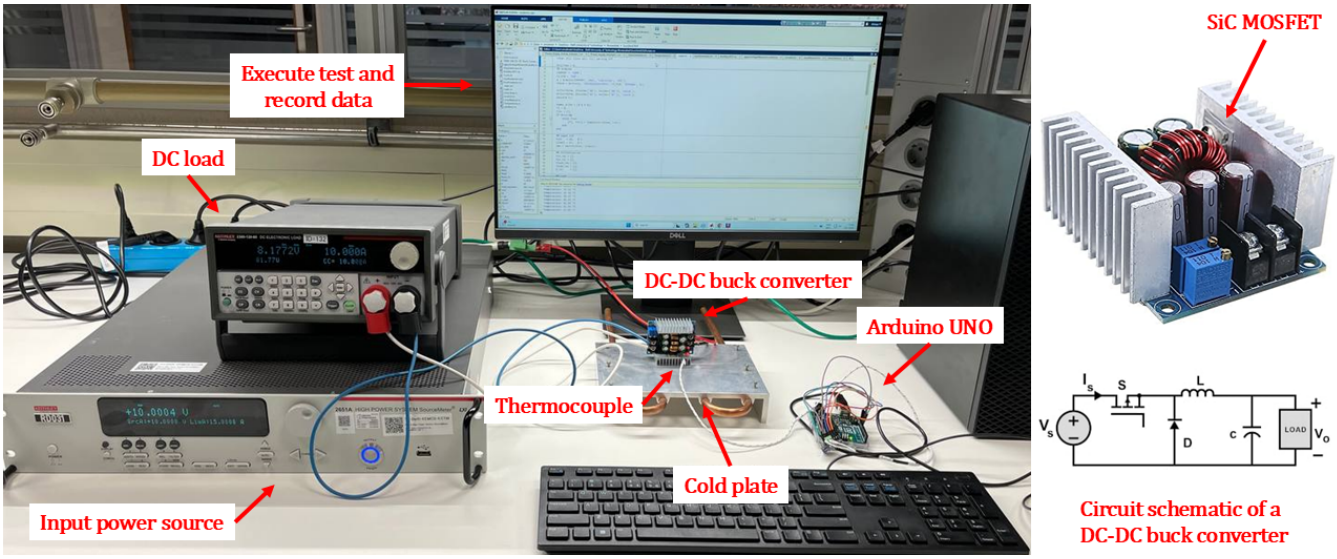


Fig. 2: Experimental setup for health monitoring of the SiC MOSFET in A DC–DC buck converter.

approach for failure detection is identifying abnormalities in the system's behavior through system identification methods. In these methods, the behavior of the system is simulated to determine how it responds to different and unseen inputs. If the system behaves differently from expectations, the abnormality can be detected. Therefore, the first step is system identification. However, detecting abnormalities and determining their sources requires accurate decision-making to avoid false alarms and to clearly interpret mixed signals when identifying the origin of the abnormality. Finally, to assess the abnormality or the level of variation in the health state of the system, parametric simulation is required to update system parameters so that they match the system after experiencing degradation or failure. This leads to a three-agent digital twin: one for system identification, one for failure detection and localization, and one for failure assessment.

This separation not only simplifies the modeling but also provides the flexibility to select the virtual domain of the first stage as a black-box model that detects failures quickly and protects the device, while allowing the final domain to include more detailed modeling that can provide more accurate feedback to a controller, even if it requires more extensive computation and longer processing time. Therefore, for the application of this concept to health monitoring of the buck converter, a temporal ANN is used in the first domain for system identification of the converter by predicting the temperature at the sensor location and the power loss of the system, where:

$$P_{loss} = V_{in} \times I_{in} - V_L \times I_L \tag{2}$$

where V_{in}, I_{in}, V_L and I_L are the input voltage and current, and the load voltage and current, respectively.

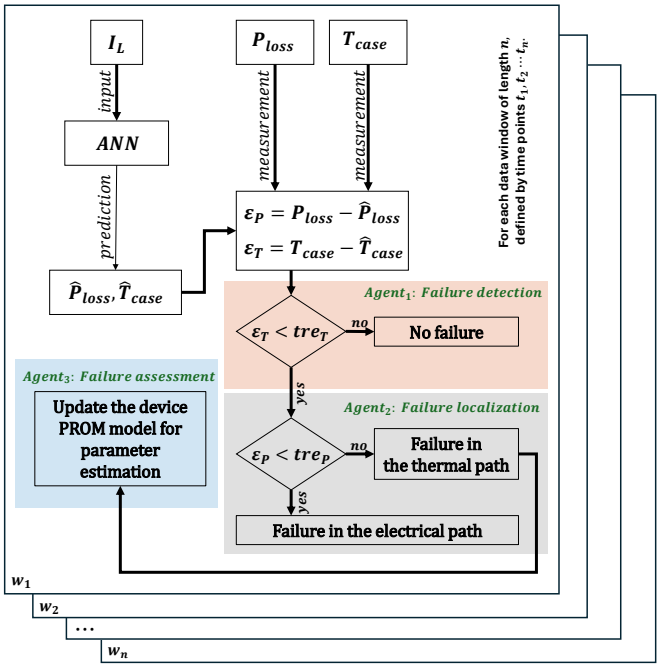


Fig. 3: Architecture of the proposed multi-agent digital twin framework, for the target of this paper.

The agent in this domain is approving the accuracy of the system identification. In the second domain, abnormality is detected based on the deviation between the expected temperature and power loss predicted by the ANN model and the measured values. If the deviation occurs only in the predicted temperature, the agent can conclude that the failure is limited to the thermal path. However, if the deviation occurs in both temperature and power loss, the agent concludes that the failure is in the electrical path. This decision is transferred to the third agent to update the parameters of a parametric

Authorized licensed use limited to: TU Delft Library. Downloaded on July 13,2026 at 13:04:58 UTC from IEEE Xplore. Restrictions apply.

model to quantify the failure. For that a PROM is selected as the virtual domain in the third stage. The flowchart of the multi-agent digital twin for this problem is shown in Fig. 3.

A. $Agent_1$: System Identification

An ANN can be trained using either a feedforward or a feedback architecture. The choice between these two largely depends on the type of data. Data can originate from static or dynamic (temporal) systems. In static systems, the relationship between the input and output is valid only at a specific time step, and feedforward ANNs are typically used for such data. However, in dynamic systems, where both inputs and outputs change over time, feedback from the output can help the model better capture the system's dynamic behavior. In these systems, time-series data from sensors can be used for both training and testing, which, to some extent, helps address the challenge of insufficient data that commonly arises during ANN training [11].

For this work, a feedback AI model called as Nonlinear Autoregressive with Exogenous Input Neural Network (NARX-ANN), is used to estimate T_{case} and P_{loss} due to the applied load, I_L.

In the literature, there are two types of NARX: open-loop NARX and closed-loop NARX. The open-loop NARX uses feedback from the true output of the previous time step as an additional input to predict the output for the next time step. The closed-loop NARX uses feedback from the predicted previous output to estimate the current output.

The open-loop NARX can be trained online and in parallel with the real device to predict the output, while the closed-loop NARX must be trained offline first.

The equation of the open-loop NARX is

$$y = F(y_{k-1}, y_{k-2}, ..., y_{k-n}, u_{k-1}, u_{k-2}, ..., u_{k-m}), \quad (3)$$

and the equation of the closed loop NARX is

$$\hat{y} = G(\hat{y}_{k-1}, \hat{y}_{k-2}, ..., \hat{y}_{k-l}, u_{k-1}, u_{k-2}, ..., u_{k-m}), \quad (4)$$

where u is the input of the system, y is the output of the system, $\hat{y}$ is the predicted output, n, l, and m are the feedback delay of the output, predicted output, and the input respectively, and F and G are nonlinear functions. This nonlinear functions can be replaced by ANNs.

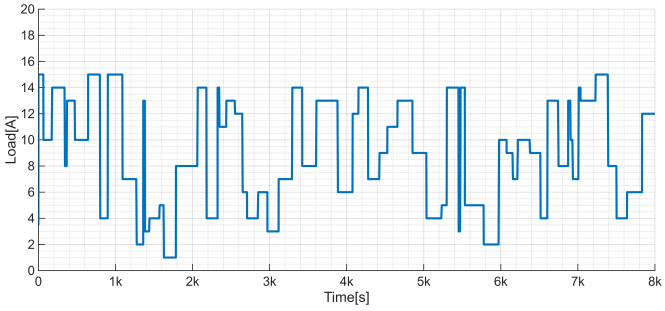
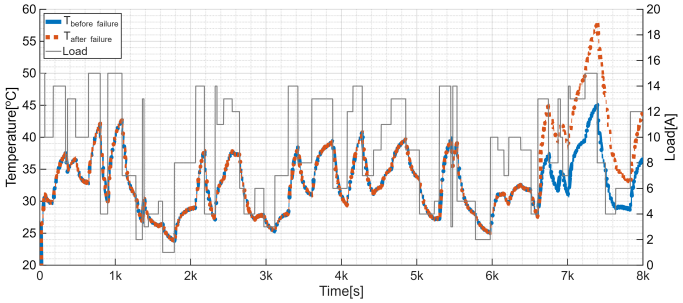
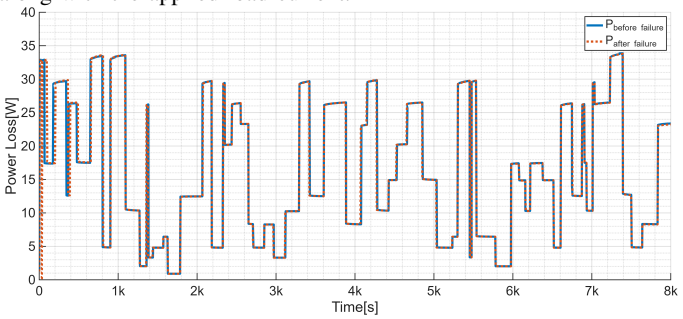


Fig. 4: Applied random load current profile.



(a) Measured temperature profiles under healthy and failure conditions, along with the applied load current.



(b) Calculated power loss under healthy and failure conditions, along with the applied load current.

Fig. 5: Measured temperature and calculated power loss under healthy and failure conditions, together with the applied load current during the experiment.

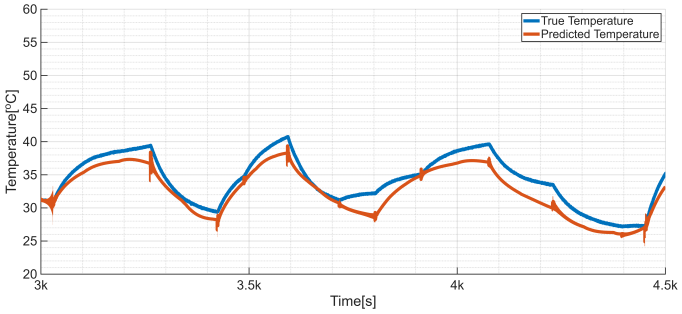
For the application presented in this paper, two different scenarios can be used to generate the required data to train the NARX-ANN. In the first scenario, the converter can be operated multiple times with a fixed but different load in each run. However, this approach requires conducting many separate tests. In addition, the transient behavior of the load would only be studied from zero to steady state and back to zero, while transitions from higher to lower loads would not be included.

As an alternative, instead of applying a fixed load and repeating the test, a randomly varying load can be applied, where both the amplitude and the duration of the load change randomly and continuously over a certain period. This type of loading is closer to real applications, such as in electric vehicles. For this reason, the second approach was selected, and the random load illustrated in Fig. 4 was applied at the output of the converter.

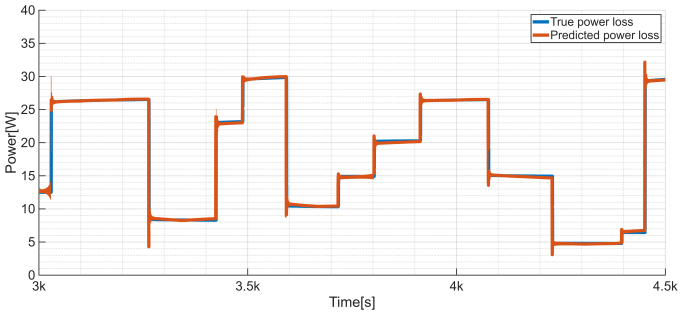
The amplitude and duration of the load change randomly between 1 A and 15 A. Using the applied load, the test was conducted twice. In the first run, the cold plate was attached to the heatsink of the converter, simulating normal operating conditions, and the test lasted for 2 hours and 20 minutes. In the second run, the cold plate was removed at 1 hour and 50 minutes after the beginning of the test to simulate a failure. The resulting measured temperature and power losses can be found in Fig. 5.

The generated experimental data were divided into three

Authorized licensed use limited to: TU Delft Library. Downloaded on July 13,2026 at 13:04:58 UTC from IEEE Xplore. Restrictions apply.



(a) Comparison between measured and NARX-ANN predicted temperature at the MOSFET sensor location.



(b) Comparison between measured and NARX-ANN predicted power loss of the converter.

Fig. 6: Predicted temperature and power loss obtained using the trained NARX-ANN during the validation period, compared with the measured values.

sections. The data points up to 3k seconds were used to train the NARX-ANN. The data from 3k to 4.5k seconds were used for validation of the NARX-ANN and for system identification in this subsection. The remaining data points were used in the next subsection for failure detection and localization, and in the final subsection for failure assessment.

For system identification, and consequently for failure or abnormality detection, the NARX-ANN was first trained using an open-loop structure. It was then fine-tuned by closing the loop of the trained open-loop NARX and retraining it for a few additional epochs. The architectures of both networks were selected similarly, with six hidden layers and 10 neurons in each layer. In addition, a delay of 10 data points was selected for both the input and output data as feedback to the input. Bayesian regularization backpropagation was chosen as the training function for both models. This method updates the weights and biases using Levenberg–Marquardt optimization. The open-loop NARX was trained for 150 epochs, while the closed-loop NARX was trained for 50 epochs. Mean Square Error(MSE) was used to evaluate the model performance during training. Fig. 6 shows the predicted temperature and power losses versus the measured values from 3k to 4.5k seconds.

In addition, the MSE between the predicted temperature and the measured temperature, as well as between the predicted power loss and the true power loss in this time domain, were calculated as $3.164\ [^oC]$ and $0.086\ [W]$, respectively. These results show that the NARX-ANN predicts both outputs with acceptable accuracy and has learned the nonlinear behavior of the converter by predicting its response when unseen inputs are applied. Therefore, it can be used for abnormality detection. This decision leads to moving to the next virtual domain, which is failure detection and localization.

B. $Agent_2$: Failure Detection and Localization

As mentioned earlier, a failure can be defined as the behavior of the device deviating from normal operating conditions. In the previous section, the behavior of the device was modeled using a NARX-ANN, meaning that the model can predict the expected temperature and power loss under applied unseen loads. Therefore, deviation between the predicted values and the measured values can indicate a failure. However, directly comparing predicted and measured values may lead to false alarms and instability in failure detection, because the NARX-ANN, like other estimation methods, predicts the true value with some error:

$$y(t) = \hat{y}(t) + \epsilon(t) \tag{5}$$

where y is the true output, $\hat{y}$ is the predicted output, and ϵ is the prediction error that represents model uncertainty and measurement noise. As shown in Fig. 6, this prediction error varies at different time steps and is not constant, which is typical in temporal ANNs. To account for this, a confidence interval is defined for ϵ based on conditions where the device is assumed to be in a healthy state. Abnormality is detected when the prediction error falls outside this health interval.

To define the interval, a distribution-free statistical characterization is adopted. This avoids restrictive assumptions that may not hold for nonlinear NARX-ANN models, (where residuals may exhibit non-Gaussian and heteroscedastic behavior). For doing so, to capture the time-varying nature of ϵ, a sliding window is defined as:

$$W_n(k) = \epsilon_n(1), \epsilon_n(2), ..., \epsilon_n(k) \tag{6}$$

where k is the window size and n is the index of the window over the sampling sequence. The threshold is then defined as the p_{th} percentile of the absolute value of ϵ within the window, where

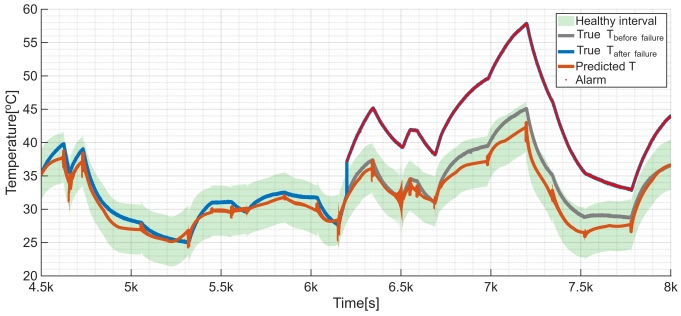
$$p = condifent \times 100 \tag{7}$$

This calculated threshold is applied as the upper and lower bounds of the health interval for failure detection.

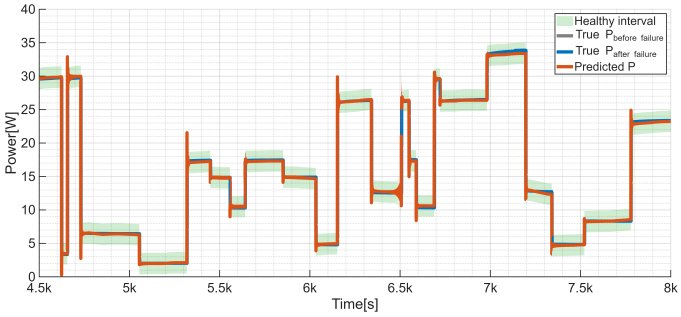
In addition, under real operating conditions, spikes or abrupt variations may appear in the data due to modeling errors, measurement noise, or transient disturbances. As a result, ϵ may exceed the defined interval and trigger an alarm. To avoid such false alarms, a persistence criterion for the alarm has been defined as:

$$\delta(j) = \begin{cases} 1 & \text{if } \epsilon > Upper\ bond \ || \ \epsilon < Lower\ bond \\ 0 & \text{otherwise} \end{cases} \tag{8}$$

Authorized licensed use limited to: TU Delft Library. Downloaded on July 13,2026 at 13:04:58 UTC from IEEE Xplore. Restrictions apply.



(a) Measured and predicted temperature during failure detection, illustrating deviation from the healthy interval and triggering of the failure alarm.



(b) Measured and predicted power loss during failure detection, remaining within the healthy interval and indicating no electrical-path failure.

Fig. 7: Failure detection results using the NARX-ANN-based, showing predicted and measured signals together with the defined health confidence interval.

Then, an alarm is triggered only if the violation persists for I consecutive samples:

$$\Sigma\delta(j)_{j=1}^{I} \geq I. \tag{9}$$

To evaluate the ability of the trained NARX-ANN for failure detection, the unseen portion of the load current (from 45k seconds until the end) was used as the input to the NARX-ANN to predict the T_{case} and P_{loss}. To define the interval, a 96% confidence level was selected for the prediction error under healthy operating conditions, with a window size of 200 time steps. In addition, to avoid false alarms, I was set to 30. Given a sampling time of 0.03 $[s]$, this means that the abnormality or out of bound error must persist for approximately 1 s to be considered a failure.

The resulting predictions are shown in Fig. 7. These results indicate that after the failure, the power loss remains unchanged, as both the predicted and the measured power losses remain within the healthy interval. However, while the predicted temperature and the expected temperature under healthy conditions remain within the healthy interval, the true measured temperature after the failure falls outside the interval. In addition, at the moment of removing the cold plate to simulate the failure, an abrupt jump occurs in the measured temperature, and $Agent_2$ correctly excludes this transient and does not raise an alarm for this jump.

Based on these observations, the deviation from the healthy interval behavior of the device can be considered a failure. Moreover, as mentioned earlier and shown in Fig. 3, since the abnormality is detected only in the temperature and not in both temperature and power loss, the failure is identified as occurring in the thermal path. This constitutes the decision of $Agent_2$.

C. $Agent_3$: Failure Assessment

Lumped-parameter thermal networks provide a method to model semiconductor devices in the form of a thermal equivalent circuit composed of elementary components such as thermal resistors, capacitors, and sources. These components represent thermal path resistances, thermal inertias, and losses, and they are connected in the form of a resistive–capacitive (RC) network. This model is used in this work to define a PROM model of the converter and to assess changes in system parameters when failure occurs [6].

To create the RC network, since detailed information about the internal layers of the MOSFET was not available, the thermal resistance and thermal capacitance of the MOSFET were selected as lumped values, representing the overall thermal resistance and capacitance of the entire MOSFET. For the same reason, the temperature of the MOSFET was assumed to be a lumped temperature. Fig. 8 shows the thermal network, where R_{MOSFET}, C_{MOSFET}, R_{th} and C_{th} represent the thermal resistance and thermal capacitance of the MOSFET and the thermal path, respectively, and all elements are referenced to the environmental temperature.

To create the PROM and derive the state-space equations of the system, Kirchhoff's current law was used. Considering fixed power loss and varying sensed temperature, the power loss was treated as the input of the system and the temperature as the output. Therefore, the equations of the system can be written as:

$$Q_{LS} = \frac{T_L - T_S}{R_M} = \frac{x_1 - x_2}{R_M} \tag{10}$$

$$Q_{SA} = \frac{T_S - T_A}{R_{Th}} = \frac{x_2}{R_{Th}} \tag{11}$$

$$C_M\ \dot{x_1} = u - Q_{SA} = u - \frac{x_1 - x_2}{R_M} \tag{12}$$

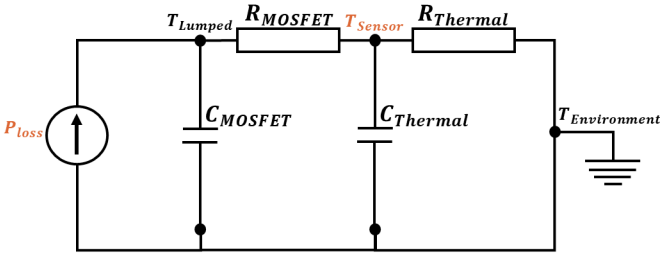


Fig. 8: RC thermal network used as the PROM for modeling.

Authorized licensed use limited to: TU Delft Library. Downloaded on July 13,2026 at 13:04:58 UTC from IEEE Xplore. Restrictions apply.

$$C_{Th}\ \dot{x_2} = u - Q_{LS} - Q_{SA} = \frac{x_1 - x_2}{R_M} - \frac{x_2}{R_{Th}} \tag{13}$$

where $x_1 = T_L - T_A$, $x_2 = T_S - T_A$, and $u(t) = P_{loss}(t)$. Here, Q_{LS}, Q_{SA}, T_L, T_S, and T_A represent the heat flow from the lumped temperature to the sensor, the heat flow from the sensor to the ambient, the lumped temperature, the measured temperature, and the ambient temperature, respectively, where the ambient temperature is considered to be 22 °C in this work. Also, R_M, C_M, R_{Th}, and C_{Th} represent the thermal resistance and capacitance of the MOSFET and the thermal path.

These equations can be rearranged as:

$$\dot{x}_1 = -\frac{1}{R_M C_M} x_1 + \frac{1}{R_M C_M} x_2 + \frac{1}{C_M} u \tag{14}$$

and,

$$\dot{x}_2 = \frac{1}{R_M C_{Th}} x_1 - (\frac{1}{R_M C_{Th}} + \frac{1}{R_{Th} C_{Th}}) x_2 + \frac{1}{C_M} u \tag{15}$$

Therefore, the state-space equations can be written as:

$$\dot{x(t)} = Ax(t) + Bu(t) \tag{16}$$

$$y(t) = Cx(t) + Du(t) \tag{17}$$

where $u(t)$ is the input of the system at time t, $x(t)$ is the state of the system at time t, and $y(t)$ is the output of the system at time t, and A, B, C, and D are the system matrices defines as:

$$A = \begin{bmatrix} -\frac{1}{R_M C_M} & \frac{1}{R_M C_M} \\ \frac{1}{R_M C_{Th}} & -(\frac{1}{R_M C_{Th}} + \frac{1}{R_{Th} C_{Th}}) \end{bmatrix},$$

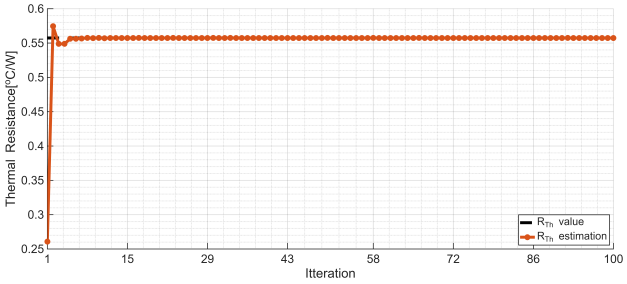
$$B = \begin{bmatrix} \frac{1}{C_M} \\ 0 \end{bmatrix},$$

$$C = \begin{bmatrix} 1 & 0 \end{bmatrix},$$

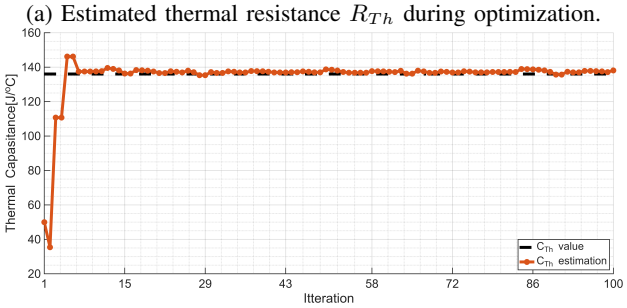
$$D = 0. \tag{18}$$

and $y = x_2$.

A nonlinear least-squares method with a maximum of 100 iterations was used to optimize R_{Th} and C_{Th} while keeping R_M and C_M fixed, in order to predict the temperature profile before and after the failure, given that the failure is applied only to the thermal path. This assumption was adopted because, as mentioned earlier, exact information about the material properties of the cold plate, heatsink, and MOSFET of the converter under study is not available. The parameter optimization was performed twice: first, to optimize the parameters of the steady-state system to match the temperature predicted by the NARX model, since the true expected temperature is not available; and second, to optimize the parameters to fit the temperature measured by the sensor after the failure.

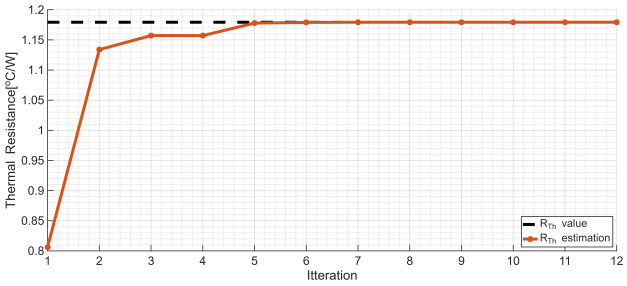


(a) Estimated thermal resistance R_{Th} during optimization.

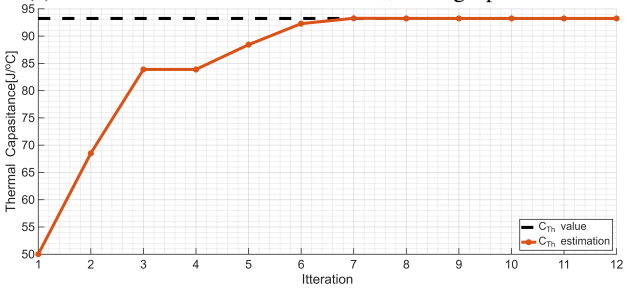


(b) Estimated thermal capacitance C_{Th} during optimization.

Fig. 9: Estimated R_{Th} and C_{Th} from predicted temperature by the NARX-ANN.



(a) Estimated thermal resistance R_{Th} during optimization.



(b) Estimated thermal capacitance C_{Th} during optimization.

Fig. 10: Estimated R_{Th} and C_{Th} from measured temperature after failure.

As the temperature profile predicted by the NARX-ANN oscillates at certain points, it was difficult for the optimizer to accurately estimate R_{Th} and C_{Th}. The optimization reached the maximum number of iterations while the estimated values were still oscillating, as shown in Fig. 9.

On the other hand, when updating the model for the post-failure condition using the measured temperature, R_{Th} and C_{Th} converged to stable values after 12 iterations (Fig. 10).

Authorized licensed use limited to: TU Delft Library. Downloaded on July 13,2026 at 13:04:58 UTC from IEEE Xplore. Restrictions apply.

Parameter	Before the failure	After the failure	Change
R_{th} $[^oC/W]$	0.5574	1.1793	+111.57%
C_{Th} $[J/^oC]$	136.032	93.235	-31.46%

TABLE I: Thermal parameters R_{Th} and C_{Th} before and after failure, showing changes in the thermal path characteristics obtained from PROM parameter estimation.

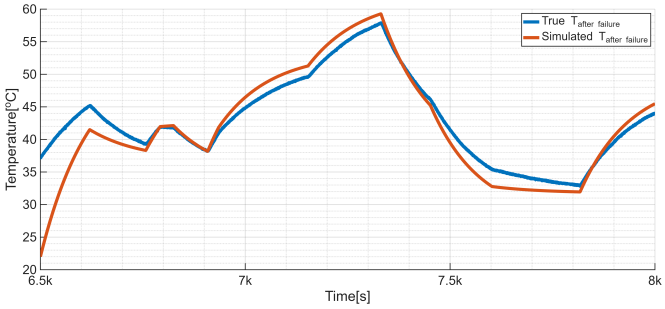


Fig. 11: Simulated temperature after failure using the updated steady-state model.

The updated parameters were then used to simulate the temperature after the failure using the updated state-space system, and the results are presented in Fig. 11. These results confirm that the parameters of the PROM have been updated from the healthy state of the system to the failure condition. This provides sufficient information for $Agent_3$ to assess the failure.

Table I shows the R_{Th} and C_{Th} values before and after the failure. It can be seen that the thermal resistance increased and the thermal capacitance decreased. The changes in these parameters are consistent with physical concepts, as temperature increases with higher thermal resistance, and the effective thermal mass decreases after removing the cold plate, resulting in reduced thermal capacitance.

IV. Conclusion

This paper introduced the concept of a multi-agent digital twin framework for modeling complex systems, demonstrated through a case study of online health monitoring of a power semiconductor in a DC–DC buck converter. The proposed approach divides the digital twin into multiple virtual domains with different roles and fidelity levels, enabling efficient monitoring, failure detection, localization, and assessment while reducing modeling complexity compared to a single comprehensive model. By structuring the digital twin as a sequence of specialized agents, the framework enables fast detection using data-driven methods and detailed failure assessment using physics-based models.

For monitoring the semiconductor, a three-agent digital twin was developed. In the first domain, a temporal ANN was used for system identification, successfully learning the nonlinear behavior of the converter and accurately predicting temperature and power loss under unseen load conditions. In the second domain, the analysis of deviations between predicted and measured signals enabled failure localization. In the third domain, a thermal PROM was used to assess and quantify the failure. By updating thermal parameters, the model captured changes in the thermal behavior of the device after experiencing failure.

Overall, the results demonstrate that the multi-agent digital twin framework provides a flexible and scalable solution for health monitoring of power electronic systems, whereas relying on a single model would make this task significantly more difficult.

Acknowledgment

Funded by the European Union (Grant Agreement No. 101072491). Views and opinions expressed are those of the author(s) only and do not necessarily reflect those of the European Union or the European Research Executive Agency. Neither the European Union nor the granting authority can be held responsible for them. Partners from the UK are supported by the UK Engineering and Physical Sciences Research Council.

References

[1] M. Awais, S. Amin, J. M. Ortega, F. P. Brito, Ó. Carvalho, N. Costa, J. L. Afonso, and V. Monteiro, "Thermal management of sic devices in high-power ev fast-charging converters: A novel proposal based on vapor chambers," *IEEE Access*, vol. 14, pp. 10305–10326, 2026.

[2] A. Dutta and S. S. Ang, "Electromagnetic interference simulations for wide-bandgap power electronic modules," *IEEE Journal of Emerging and Selected Topics in Power Electronics*, vol. 4, no. 3, pp. 757–766, 2016.

[3] Y. Fan, H. Qian, H. Liu, Y. Wang, W. Zhu, and L. Wang, "Electro-thermo-mechanical simulation analysis of multichip sic mosfet power modules," in *2024 25th International Conference on Electronic Packaging Technology (ICEPT)*, pp. 01–06, IEEE, 2024.

[4] M. Musadiq, A. Inamdar, R. Roucou, and W. D. Van Driel, "Investigating competing failure modes in microelectronic devices due to small temperature variations," in *2024 IEEE 10th Electronics System-Integration Technology Conference (ESTC)*, pp. 1–6, IEEE, 2024.

[5] M. Yun, D. Yang, M. Cai, H. Yan, J. Yu, M. Liu, S. He, and G. Zhang, "Aging and sintered layer defect detection of discrete mosfets using frequency domain reflectometry associated with parasitic resistance," *IEEE Transactions on Device and Materials Reliability*, vol. 24, no. 1, pp. 129–141, 2024.

[6] B. Rodriguez, E. Sanjurjo, M. Tranchero, C. Romano, and F. Gonzalez, "Thermal parameter and state estimation for digital twins of e-powertrain components," *IEEE Access*, vol. 9, pp. 97384–97400, 2021.

[7] L. Thibault, P. Avitabile, J. Foley, and J. Wolfson, "Equivalent reduced model technique development for nonlinear system dynamic response," *Mechanical Systems and Signal Processing*, vol. 36, no. 2, pp. 422–455, 2013.

[8] Y. J. Cruz, F. Castano, A. Villalonga, M. Mishra, and R. E. Haber, "A data-driven approach for predicting remaining useful life of semiconductor devices based on machine learning and synthetic data generation. a review and case study on sic mosfets," *IEEE Access*, 2025.

[9] A. Inamdar, W. D. van Driel, and G. Zhang, "Digital twin technology—a review and its application model for prognostics and health management of microelectronics," *Electronics*, vol. 13, no. 16, p. 3255, 2024.

[10] E. Glaessgen and D. Stargel, "The digital twin paradigm for future nasa and us air force vehicles," in *53rd AIAA/ASME/ASCE/AHS/ASC structures, structural dynamics and materials conference 20th AIAA/ASME/AHS adaptive structures conference 14th AIAA*, p. 1818, 2012.

[11] A. Mehrabi, K. Yari, W. D. Van Driel, and R. H. Poelma, "Ai-driven digital twin for health monitoring of wide band gap power semiconductors," in *2024 IEEE 10th Electronics System-Integration Technology Conference (ESTC)*, pp. 1–8, IEEE, 2024.

Authorized licensed use limited to: TU Delft Library. Downloaded on July 13,2026 at 13:04:58 UTC from IEEE Xplore. Restrictions apply.